Journal of Solid State Chemistry 182 (2009) 813–820

Contents lists available at ScienceDirect

Journal of Solid State Chemistry

journal homepage: www.elsevier.com/locate/jssc

Electronic properties and rare-earth ions photoluminescence behaviors in borosilicate: $SrB_2Si_2O_8$

Yuhua Wang [a,b,*], Zhiya Zhang [a], Jiachi Zhang [a], Yanghua Lu [c]

[a] Department of Materials Science, School of Physical Science and Technology, Lanzhou University, Lanzhou 730000, PR China
[b] Key Laboratory for Magnetism and Magnetic Materials of the Ministry of Education, Lanzhou University, Lanzhou 730000, PR China
[c] Shenzhen Star Optoelectronic Technology Co. Ltd, Shenzhen 518101, PR China

ARTICLE INFO

Article history:
Received 16 September 2008
Received in revised form
3 January 2009
Accepted 7 January 2009
Available online 19 January 2009

Keywords:
Rare earth ion
$SrB_2Si_2O_8$
Reduction in air
UV–VUV
Host lattice absorption

ABSTRACT

Undoped and *RE* ions doped $SrB_2Si_2O_8$ were successfully synthesized. After the application of UV and VUV spectroscopy measurements, we made a novel discovery that the emission of $SrB_2Si_2O_8$:Eu prepared in air can be switched between red and blue by the different excitations. The information is that quite a part of Eu^{3+} was spontaneously reduced to Eu^{2+} in air. The PL properties of Eu^{2+} in VUV and Eu^{3+}, Ce^{3+} and Tb^{3+} in UV–VUV region in $SrB_2Si_2O_8$ were evaluated for the first time. The excitation mechanisms of the O^{2-}–Eu^{3+} CT, Ce^{3+} *f–d* and Tb^{3+} *f–d* transitions in UV region as well as the Eu^{3+} *f–d*, O^{2-}–Ce^{3+} CT, O^{2-}–Tb^{3+} CT transitions and the host lattice absorption in VUV region were established. In addition, first principles calculation within the LDA of the DFT was applied to calculate the electronic structure and linear optical properties of $SrB_2Si_2O_8$ and the results were compared with the experimental data.

1. Introduction

Danburite ($CaB_2Si_2O_8$) is a naturally-occurring alkali borosilicate mineral. It is a crystalline analog of borosilicate glass, which is matrix of choice for confinement of high-level radioactive waste [1]. The crystal structure of $CaB_2Si_2O_8$ has been studied [2–4] and refined by Phillips [3] and Downs [4] in their investigations of the single-crystal X-ray diffraction (XRD) measurements. Also, $CaB_2Si_2O_8$ is an attractive system considering the problem of chemical bonding in ionic crystals within the quantum theory of atoms in molecules (AIM) [5,6]. The topology of the electron density in $CaB_2Si_2O_8$ was both experimentally and theoretically studied by Downs [4] and Luaña [7], respectively. From the above investigations of the structure, we know that $CaB_2Si_2O_8$ possesses a rigid crystal structure. Note that it was the natural $CaB_2Si_2O_8$ crystal that employed in all the previous studies. In 1979, Gaft and coworkers [8] firstly reported the ultraviolet (UV) photoluminescence (PL) properties of rare-earth (*RE*) ions in both natural and a hydrothermally synthesized $CaB_2Si_2O_8$. To the best of our knowledge, no further work was published thereafter on the PL properties of $CaB_2Si_2O_8$ although several other researchers [9–11] referred to the Gaft's results in their studies. In the literature [9], the PL behaviors of Ce^{3+} in up to 366 substances were summarized and a relatively small stokes shift (ΔS) of 1805 cm^{-1} for the Ce^{3+} in $CaB_2Si_2O_8$ was presented. This value is close to those in YPO_4 (1673 cm^{-1}), YBO_3 (1881 cm^{-1}), $GdBO_3$ (1907 cm^{-1}), $YAl_3(BO_3)_4$ (1470 cm^{-1}) and $YGd_3(BO_3)_4$ (1664 cm^{-1}), all of which have been established to be excellent hosts for PL materials [12–14]. It is known that the smaller ΔS always implies the stiffer host lattice and less nonradiative relaxation after the luminescent ions are excited. So the small ΔS in $CaB_2Si_2O_8$ demonstrates the rigidity of the crystal lattice. We can attribute the rigidity to the small radius and high charge of B^{3+} as well as the crystal geometry characteristics. However, for some unknown reasons, it is difficult to prepare this compound artificially [2]. In the present work, we also did not synthesize it successfully.

$SrB_2Si_2O_8$ is another danburite [15] that also possesses an orthorhombic structure with the space group of *Pnam* (no. 62). Similar to $CaB_2Si_2O_8$, $SrB_2Si_2O_8$ has eight crystallographic sites: Sr (4*c*), B (8*d*), Si (8*d*), O1 (8*d*), O2 (8*d*), O3 (8*d*), O4 (4*c*) and O5 (4*c*). In 1972, Verstegen and colleagues [2] firstly reported the PL properties of Eu^{2+} (5 mol%)-doped $SrB_2Si_2O_8$ prepared in a reducing atmosphere. Their work is the only report on the spectroscopy in $SrB_2Si_2O_8$ we have found so far. Even though their report was just a short "Notes" and far from systematical study and detailed description, their data implied that $SrB_2Si_2O_8$:Eu^{2+} was an excellent PL phosphor with the quantum efficiency higher than 40% under 254 nm excitation.

Vacuum ultraviolet (VUV, $\lambda < 200$ nm) spectroscopy of *RE* ions has been intensely investigated because of the emerging needs for applications of the VUV-excited phosphors in such as mercury-free fluorescent tubes, plasma displays panels (PDPs) and liquid

* Corresponding author at: Department of Materials Science, School of Physical Science and Technology, Lanzhou University, Lanzhou 730000, PR China.
Fax: +86 931 8913554.
E-mail address: wyh@lzu.edu.cn (Y. Wang).

0022-4596/$ - see front matter © 2009 Elsevier Inc. All rights reserved.
doi:10.1016/j.jssc.2009.01.006

crystal display (LCD) backlights [16–19]. VUV photons have higher energy than UV photon and always excite the host lattice followed by an energy transfer process from the host to the luminescent center. Considerable interest and research activities have been focused on the efficient excitations of the host and a better understanding of the possible energy transfer channels [20–24].

Our goal in this work is to provide a complete characterization of the PL spectroscopy and clarify the possible excitation mechanisms of *RE* ions in $SrB_2Si_2O_8$ in both UV and VUV region. To this end, we have performed the techniques of reflection, UV and VUV spectroscopy. In addition, the electronic structure and the linear optical property of $SrB_2Si_2O_8$ were calculated on the basis of local density approximation (LDA) of the density-functional theory (DFT) and the results were compared with the experimental data.

2. Experimental methods and computational details

Strontium carbonate ($SrCO_3$, 99%), boracic acid (H_2BO_3, 99.5%), silicic acid (H_2SiO_3, 99%), europium oxide (Eu_2O_3, 99.99%), cerium oxide (CeO_2, 99.99%) and terbium oxide (Tb_4O_7, 99.99%) were employed as the starting materials to prepare $SrB_2Si_2O_8$ and $SrB_2Si_2O_8$:*RE* (*RE* = Eu^{3+}, Eu^{2+}, Ce^{3+}, Tb^{3+}) via a solid state reaction method. The raw materials were weighed and mixed together before sintering at 900–950 °C for 8 h in air for the Eu^{3+} doped samples. The Eu^{2+}, Ce^{3+} and Tb^{3+} doped samples were prepared in a reducing atmosphere of 5% H_2–95% N_2.

The phase purity of the samples was checked by XRD using Rigaku D/Max-2400 X-ray diffractometer with Cu*K*α radiation. The PL excitation and emission spectra were measured using an Edinburgh Instruments FLS920T. The scan speed is 30 nm/s with the step of 1 nm. The dwell time is 0.2 s. The UV spectra were measured by steady-state spectrophotometer with Xe900 (450 W xenon arc lamp) as the excitation source. The slit is 0.18 nm for the excitation and 0.8 nm for the emission spectra. The VUV light source of the spectrometer system is a 150 W Deuterium lamp (Cathodeon Inc.). The emission and excitation spectra were measured by the vacuum monochromator (VM504, Acton Research Co., ARC). The slits for the excitation and the emission spectra are 0.18 and 2 nm, respectively. The VUV excitation spectra were corrected by dividing the excitation intensity of sodium salicylate under the same measurement condition. The reflection spectrum was performed on LAMBDA 950 (Perkin Elmer, PE) with barium sulfate ($BaSO_4$) as the reference. All the spectra were recorded at room temperature.

All the calculations in the present work were based on the LDA approximation of the DFT theory [25,26]. CASTEP [27,28], used in the present work is on the basis of planewaves and pseudopotentials. The wave functions described only the valence and the conduction electrons, and the core electrons were taken into account using pseudopotentials. The preconditioned conjugate gradient (CG) band-by-band method and the Pulay density mixing scheme were used throughout the calculation to ensure an efficient way to search for the energy minimum of the electronic structure ground state. The optimized pseudopotential [29] in the Kleinman-Bylander form [30,31] allowed us to use a small plane-wave basis set and simultaneously meet the accuracy required by our current study. The configuration of $SrB_2Si_2O_8$ employed in the calculation was from the reported data in the literature [15]. The considered valence electrons for Sr, B, Si and O were $4s^24p^65s^2$, $2s^22p^1$, $3s^23p^2$ and $2s^22p^4$, respectively. The Read and Needs correction [32] was applied to ensure accurate optical matrix elements calculations for our nonlocal pseudopotential based method. A scissors operator [33] is usually introduced to shift all the conduction bands to ensure that the calculated result is consistent with the measured one. A kinetic-energy cutoff of 450 ev was used throughout the calculation and its reliability were further demonstrated in the result of the linear optical property calculation.

3. Crystal structure of $SrB_2Si_2O_8$

Fig. 1 exhibits the DIAMOND [34,35] drawn crystal structure of $SrB_2Si_2O_8$ according to the atomic coordinates reported in the literature [15]. It can be found that the structure viewed along [010] in Fig. 1a is similar to that of $CaB_2Si_2O_8$ along [001] [3,4]. The framework is based on four-membered rings of corner-sharing BO_4 and SiO_4 tetrahedra. The Sr is located in the large cavity of the eight-membered rings and prefers to be bonded to seven oxide ions. The nearest Sr–Sr distance is 4.585 Å. As shown in Fig. 1b, the four-membered rings and the eight-membered rings form the layer (denoted as L). Between the two layers are the B_2O_7 and Si_2O_7 ditetrahedra, as exhibited in Fig. 1c.

All the prepared $SrB_2Si_2O_8$:*RE* (*RE* = Eu^{3+}, Eu^{2+}, Ce^{3+}, Tb^{3+}) samples are characterized to be single phase $SrB_2Si_2O_8$ of orthorhombic structure with the space group of *Pnam* (no. 62). The typical XRD pattern is shown in Fig. 2 and all the diffraction peaks can be well indexed based on the JCPDS No. 25-1288.

4. UV PL properties of $SrB_2Si_2O_8$:*RE* (*RE* = Eu, Ce, Tb)

4.1. UV PL properties of $SrB_2Si_2O_8$:Eu

In our experiment, we observed an interesting result that $SrB_2Si_2O_8$:Eu prepared in air exhibited both Eu^{3+} and Eu^{2+} emissions, on which we firstly reported. Fig. 3 shows the typical emission spectra. The line emissions in 580–750 nm range with

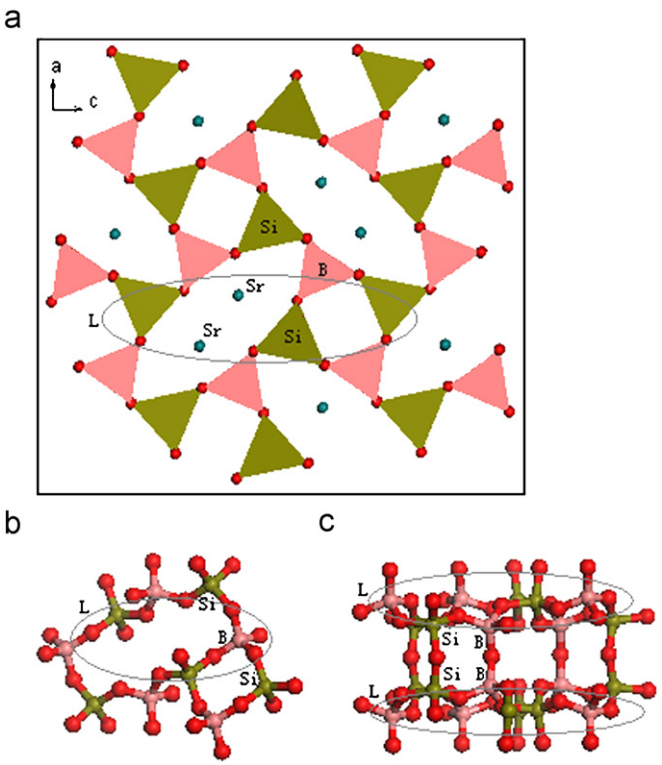

Fig. 1. The crystal structure of $SrB_2Si_2O_8$ viewed down [010] (a); the layer (L) of the eight-membered rings and the four-membered rings (b); the Si_2O_7 and B_2O_7 building units between the two layers (c).

the maximum at about 611 nm are from the Eu^{3+} centers and the band around 440 nm is the typical Eu^{2+} luminescence. The emission can be switched between the red and the blue by different excitations: under 254 nm excitation the Eu^{3+} red emission is dominant while under 365 nm the Eu^{2+} blue emission presides over the emission spectra; when excited by 340 nm the sample emits almost the pure blue; and when excited by 395 nm the two emissions present nearly equivalent intensity. The excitation spectra monitoring the Eu^{3+} (611 nm) and the Eu^{2+} (440 nm) emissions are shown in Fig. 4. The broad band around 250 nm is due to the O^{2-}–Eu^{3+} charge transfer (CT) transition and the sharp peaks between 280 and 400 nm are from the Eu^{3+} *f–f* transitions. The excitations as indicated at about 295, 340, 365, 387 and 395 nm are the crystal field splitting of the Eu^{2+} 4*f*–5*d* transition.

All these results indicate that considerable amount of Eu^{3+} in $SrB_2Si_2O_8$ were spontaneously reduced to Eu^{2+} even in air, although usually reducing atmosphere such as H_2/N_2, CO or NH_3 is necessary for the reduction. The similar phenomena were reported in natural datolite ($CaB(OH)SiO_4$) [8] and in other hosts such as SrB_4O_7 [36–38], SrB_6O_{10} [39], $SrBPO_5$ [40], $Sr_3(PO_4)_2$ [41] and $S_2B_5O_9Cl$ [42]. Four necessary conditions for reduction of trivalent *RE* ions in air were proposed by previous researchers [36,41,42]: (1) there are no oxidizing ions in the host; (2) the doped trivalent *RE* ion must substitute for the unequal valent cation in the host, such as divalent alkali earth ions; (3) RIGID three-dimensional network structure of anions exist in the composite oxide matrices; (4) RE^{2+} has similar ionic radii to that of substituted cation. As discussed previously, the Sr^{2+} in $SrB_2Si_2O_8$ are located in the rigid framework of corner-sharing BO_4 and SiO_4 tetrahedra. The ionic radius of Eu^{2+} (coordination number (CN) = 7, 134pm) is close to that of Sr^{2+} (CN = 7, 135pm). According to the above requirements, when the Eu^{3+} substitutes the Sr^{2+} in $SrB_2Si_2O_8$, reduction of Eu^{3+} to Eu^{2+} occurs in air. The reduction mechanism is thought to be the same as that proposed in the literatures [36,41,42]: when Eu^{3+} substituted for the Sr^{2+},

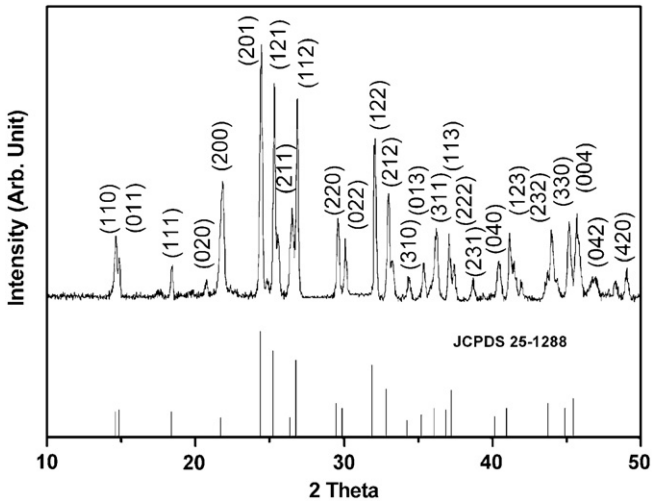

Fig. 2. XRD pattern of $SrB_2Si_2O_8$.

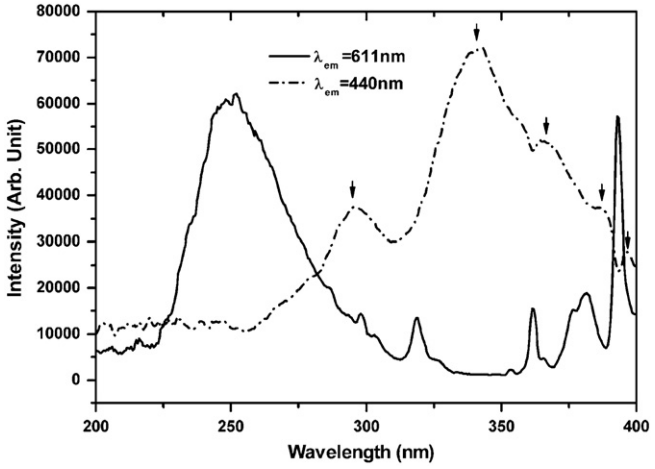

Fig. 4. Excitation spectra of $SrB_2Si_2O_8$:0.30Eu prepared in air monitoring the emissions of 611 nm (solid line) and 440 nm (dash dot line).

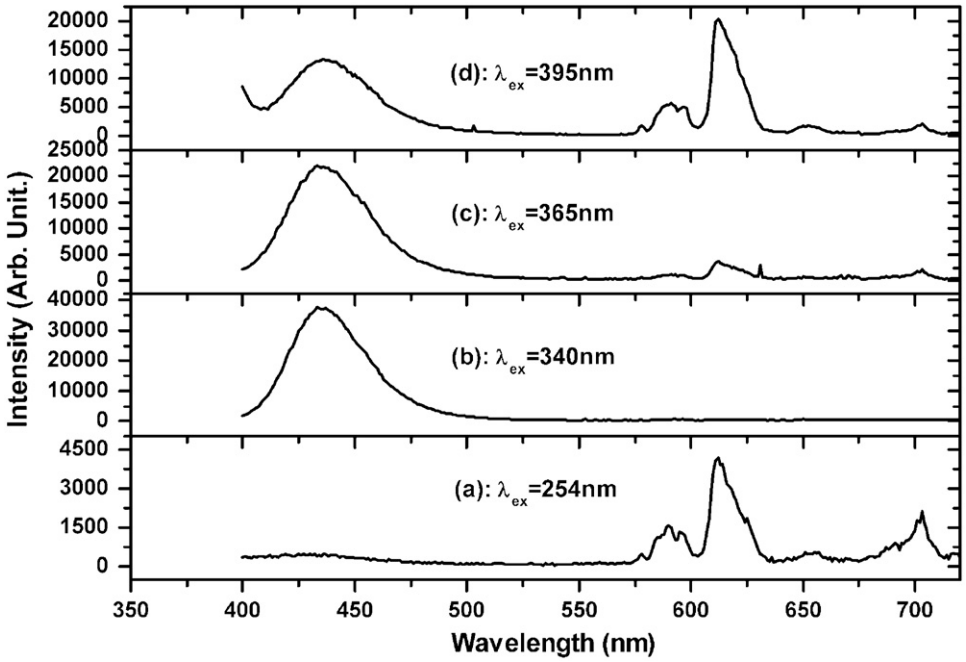

Fig. 3. Emission spectra of $SrB_2Si_2O_8$:0.30Eu prepared in air under different excitation wavelengths: (a) $\lambda_{ex} = 254$ nm; (b) $\lambda_{ex} = 340$ nm; (c) $\lambda_{ex} = 365$ nm; (d) $\lambda_{ex} = 395$ nm.

two Eu^{3+} would substitute for three Sr^{2+} in order to keep the electroneutrality of the compound; therefore, negative Sr^{2+} vacancies would be created and then be transferred to the Eu^{3+} centers by thermally stimulation movement and the Eu^{3+} were reduced to Eu^{2+}. It is worth mentioning that the results are of high repeatability. We also carried out the experiment in a N_2 or Xe atmosphere and obtained the same results. Maybe the return conversion process $Eu^{2+} \rightarrow Eu^{3+}$ in $SrB_2Si_2O_8$ can take place under some other conditions, perhaps in a much stronger oxidizing atmosphere. However, it needs further experimental evidence.

The excitation intensity ratio of the maximum at 340 nm to that at 250 nm in Fig. 4 is defined as r(B/R). We observed that r(B/R) was not dependent on the nominal Eu^{3+}-doping content or the calcination time but it exhibited a relatively higher value in $Sr_{1-3x/2}B_2Si_2O_8$:xEu (sample 1) than in $Sr_{1-x}B_2Si_2O_8$:xEu (sample 2). The result seems imply that the Eu^{3+} in sample 1 is more prone to be reduced to Eu^{2+} than in sample 2. The most acceptable explanation is that: in sample 1 two Eu^{3+} substituted for three Sr^{2+} while in sample 2 one Eu^{3+} substituted for one Sr^{2+}, so more Sr^{2+} vacancies that are negative in nature formed in sample 1 and more Eu^{3+} were reduced to Eu^{2+}. The detailed mechanisms need further investigation.

The $SrB_2Si_2O_8$:Eu^{2+} prepared in the reducing atmosphere exhibited the pure blue emission of 440 nm. The excitation spectrum is shown in Fig. 5. Obvious discrepancy between Figs. 4 and 5 can be observed, even monitored with the same wavelength of 440 nm. The result indicates that the crystal field environment surrounding the Eu^{2+} has changed to certain extent in the $SrB_2Si_2O_8$:Eu^{2+} prepared in a reducing atmosphere compared with that in the $SrB_2Si_2O_8$:Eu prepared in air. We observed more splitting components for the later, in which the Eu^{2+} and Eu^{3+} are concurrent and the local crystallographic environment around the Eu^{2+} may be perturbed by the Eu^{3+} centers or other defects. This observation supports the important inductive effect in solid state chemistry [43]: in inorganic compounds, when a second cation T is present, it will modify the character of the bond between the existing cations (M) and anions (X), i.e. the T has an inductive effect on the M–X bond.

The quenching concentration of Eu^{2+} in $SrB_2Si_2O_8$:Eu^{2+} was determined to be 30 mol%, a relatively high value as indicated in the inset of Fig. 5. In $SrB_2Si_2O_8$:Eu^{2+}, the Eu^{2+} are supposed occupy the Sr^{2+} sites and locate in the large cavity of the framework as shown in Fig. 1. The energy transfer between the Eu^{2+} centers would be hindered so that the Eu^{2+} emission possesses a high quenching concentration. The large Sr–Sr distance as discussed previously may also reduce the energy transfer probability between the Eu^{2+} centers when Eu^{2+} occupied the Sr^{2+} sites.

4.2. UV PL properties of $SrB_2Si_2O_8$:Ce^{3+}

The curves (a) and (b) in Fig. 6 show the emission and excitation spectra of $SrB_2Si_2O_8$:0.05Ce^{3+}, respectively. In curve (a), the broad-band emission around 396 nm is attributed to the transition from the lowest 5d level to the ground state ^2F ($4f^1$) of Ce^{3+}. We cannot distinguish the spin-orbit split $^2F_{5/2}$ and $^2F_{7/2}$ from the broad band. By using a Gaussian least-square fit, the broad band (curve (c)) is deconvoluted into two sub-bands with the maxima at 390 nm (curve (d)) and 421 nm (curve (e)). The two sub-bands are responsible for the Ce^{3+} 5d-^2F_J ($J = 7/2$, 5/2) transitions, respectively. Accordingly, the ^2F_J ($J = 7/2$, 5/2) energy gap of Ce^{3+} in $SrB_2Si_2O_8$ is estimated to be 1888 cm^{-1}. This value is similar to those observed in other Ce^{3+} activated phosphors [41,44,45].

The lowest $4f^{n-1}5d$ energy of lanthanide ion (Ln) in host A is denote as E(Ln, A) and that of the free Ln as E(Ln, *free*). The energy difference between E(Ln, A) and E(Ln, *free*), called crystal field depression D(Ln, A), is always a characteristic of the host. In curve (b), we observe the three lowest Ce^{3+} 5d components at 320, 295 and 250 nm in $SrB_2Si_2O_8$, respectively. Among them, the mentioned 320 nm (31 250 cm^{-1}) can be regarded as the E(Ce^{3+}, $SrB_2Si_2O_8$). The E(Ce^{3+}, *free*) was reported to be 49 340 cm^{-1} previously [46]. Accordingly, the crystal field depression D(Ce^{3+}, $SrB_2Si_2O_8$) is calculated to be 18 090 cm^{-1}.

4.3. UV PL properties of $SrB_2Si_2O_8$:Tb^{3+}

The curves (a) and (b) in Fig. 7 are the emission and excitation spectra of $SrB_2Si_2O_8$:0.05Tb^{3+}, respectively. The Tb^{3+} in $SrB_2Si_2O_8$ exhibits a green emission with the maximum at about 541 nm ($^5D_4$–$^7F_2$ transition). The excitation spectrum contains two bands at around 266 nm (37 590 cm^{-1}) and 240 nm (41 666 cm^{-1}), which are due to the transitions from the Tb^{3+} $^7F_6$ ($4f^8$) ground state to the $^9D_5$ and $^7D_5$ ($4f^7 5d^1$) excited states, respectively. The two transitions correspond to the Tb^{3+} lowest spin-forbidden and spin-allowed f–d transitions, respectively.

According to the previous investigations [46–48], the 5d states of Ln can be well predicted from that of Ce^{3+} in the same compound:

$$D(\mathrm{Ln}, A) = E(\mathrm{Ln}, \mathit{free}) - E(\mathrm{Ln}, A) \quad (1)$$

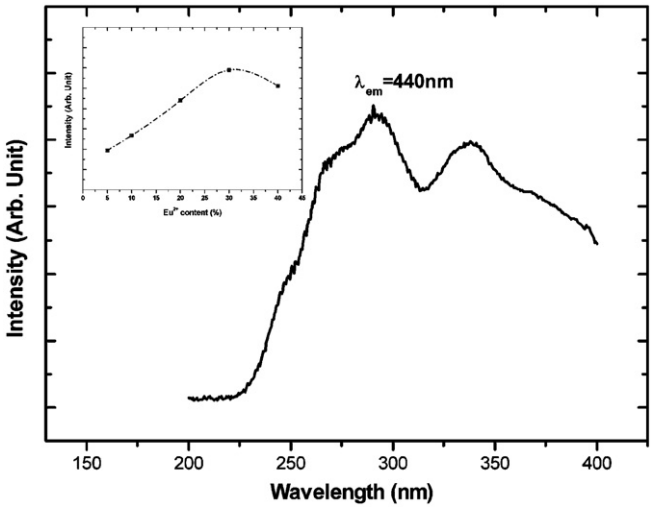

Fig. 5. Excitation spectra of $SrB_2Si_2O_8$:Eu^{2+}; the inset indicates the dependence of the 440 nm emission under 340 nm excitation on the Eu^{2+}-content.

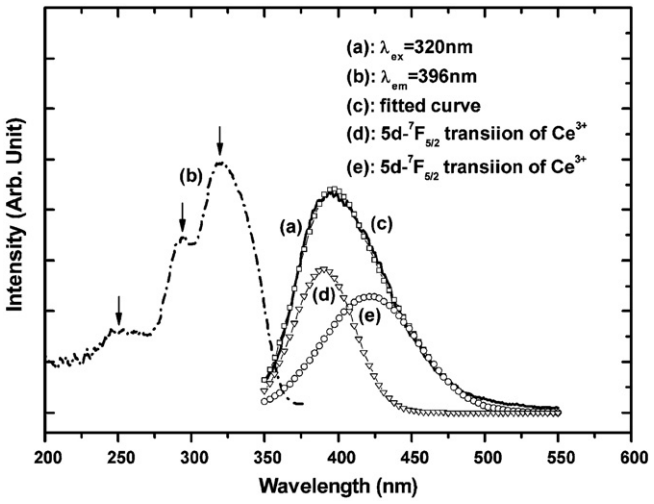

Fig. 6. Emission (a) and excitation (b) spectra of $SrB_2Si_2O_8$:0.05Ce^{3+}; (c) is the fitted curve of (a); (d) and (e) are the deconvoluted curves of (a).

As discussed above, the $D(Ce^{3+}, SrB_2Si_2O_8)$ was calculated to be 18 090 cm^{-1}. The lowest spin-forbidden and spin-allowed *f–d* transitions of free Tb^{3+} were reported to be 56 350 and 62 500 cm^{-1}, respectively [46]. By applying Eq. (1), the lowest spin-forbidden and spin-allowed *f–d* transitions for Tb^{3+} in $SrB_2Si_2O_8$ can be calculated to be 38 260 and 44 410 cm^{-1}, respectively. We find a small gap between these calculated values and the experimental results discussed in Fig. 7b.

5. Electronic and VUV PL properties of $SrB_2Si_2O_8$:*RE* (*RE* = Eu, Ce, Tb)

The curves (a)–(d) in Fig. 8 exhibit the VUV excitation spectra monitoring the Eu^{3+} (611 nm), Eu^{2+} (440 nm), Ce^{3+} (396 nm) and Tb^{3+} (541 nm) emissions, respectively. The excitation above 200 nm has been previously discussed in the UV excitation spectra and that below 200 nm will mainly be focused on here.

In Fig. 9 are plotted the experimental reflection spectrum and the theoretical absorption curve. The experimental reflection spectrum indicates that the host lattice absorption should start at about 200 nm. We find the theoretical result agrees well with the experiment. In Fig. 8, we observe the excitation between 165 and 200 nm for all the samples with the different *RE* ions, which could be accordingly assigned to the host lattice absorption of $SrB_2Si_2O_8$. The absorption of Si–O group was generally observed below 190 nm [49–52] and that of B–O group to be around 150–160 nm [53,54]. So our results were in good accordance with the reported data. Further information in the excitation spectra could be partly collected from the calculated band structure and the electron density of states (DOS) and partial electron density of states (PDOS).

Fig. 10 exhibits the direct LDA band gap energy (E_g) of 4.27 eV at G, and the indirect E_g values of 5.13, 5.72, 5.27, 5.97, 5.32, 5.85 and 6.19 eV at Z, T, Y, S, X, U and R, respectively. The calculated DOS and PDOS of $SrB_2Si_2O_8$ in Figs. 11 and 12 convey the obvious

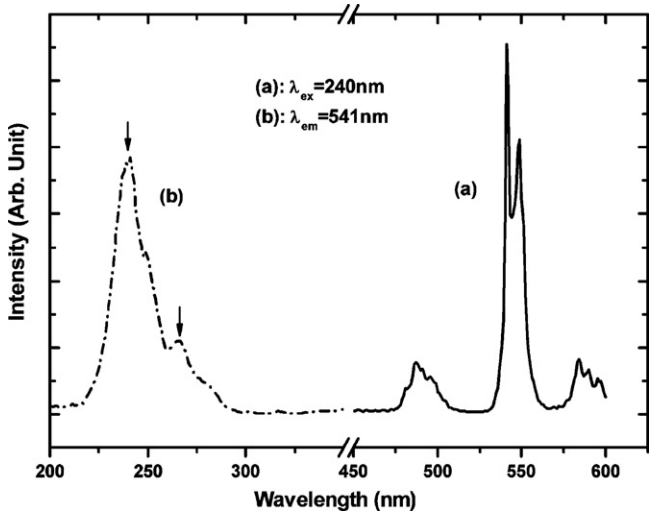

Fig. 7. Emission (a) and excitation (b) spectra of $SrB_2Si_2O_8$:0.05Tb^{3+}.

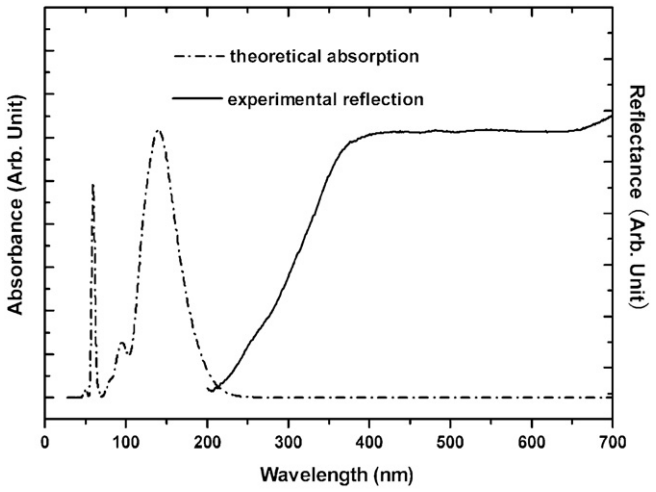

Fig. 9. Experimental reflection spectrum (solid line) and theoretical absorption curve (dash dot line) of $SrB_2Si_2O_8$.

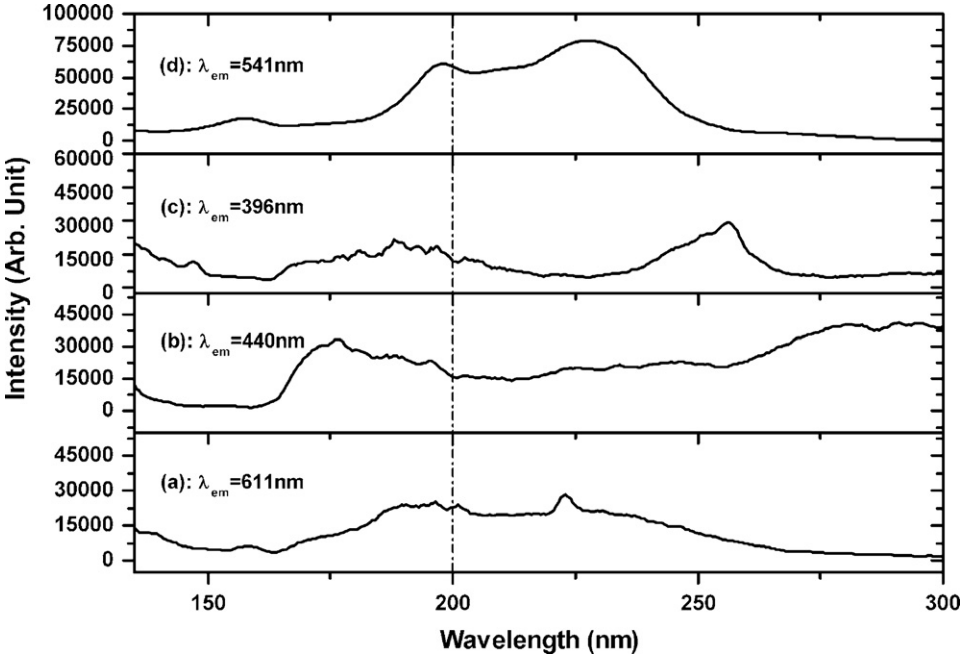

Fig. 8. VUV excitation spectra monitoring the emissions of 611 nm (a); 440 nm (b); 396 nm (c); 541 nm (d).

information that: (1) the valence band mainly stems from the O 2*p* orbitals, the VSi 3*p*(3*s*) and the B 2*p*(2*s*) orbitals hybridize with the O 2*p* orbitals and contribute to the valence band; (2) the conduction band is mainly composed of the Sr (4*s*+5*s*) orbitals, and also partly derived from the Si (3*p*+3*s*) as well as the B 2*p*(2*s*) orbitals; (3) the Si–O and B–O bonds are mainly covalent while the Sr–O bond is highly ionic in character. The recorded energy of our VUV spectrometer is above 120 nm (10.3 eV), so the electron states about −6–0 eV near the top of valence band should correspond to the VUV absorption of $SrB_2Si_2O_8$. From the above discussed DOS and PDOS of $SrB_2Si_2O_8$, we presume that the O (2*p*), Si 3*p*(3*s*), B 2*p*(2*s*) in the valence band and Si (3*p*+3*s*), B 2*p*(2*s*), Sr (4*s*+5*s*) in the conduction band are mainly involved in the VUV excitation spectra in Fig. 8. In addition, since Sr orbitals contribute remarkably to the bottom of the conduction band, the exciton would be formed near the Sr–O bond when the host was excited with high energy VUV photons. Consequently, the exciton energy responds to the high absorption intensity in the vicinity of 200 nm in Fig. 8. Note that the simplified form such as Si 3*p*(3*s*) means Si 3*p* plays a major role, and Si (3*p*+3*s*) means Si 3*p* and Si 3*s* make almost equally contribution.

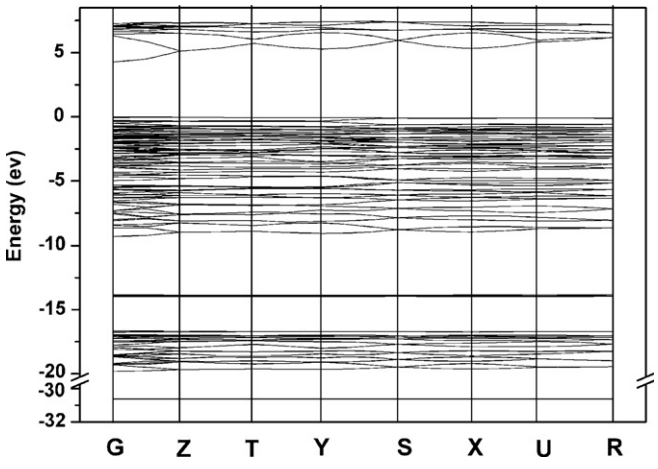

Fig. 10. Calculated band structure of $SrB_2Si_2O_8$.

The low energy 5*d* states of Ce^{3+} and Tb^{3+} in $SrB_2Si_2O_8$ were previously discussed in Figs. 6b and 7b, respectively. Their higher energy states are considered to be involved below 200 nm in curves (c) and (d), respectively. In addition, the Eu^{3+} *f*–*d*, O^{2-}–Ce^{3+} CT and O^{2-}–Tb^{3+} CT transitions in $SrB_2Si_2O_8$ can be estimated through the following calculation. The $D(Ce^{3+}, SrB_2Si_2O_8)$ was determined to be 18 090 cm^{-1} in the previous discussion. Using $E(Eu^{3+}, free)$ of 85 250 cm^{-1} [47], the $E(Eu^{3+}, SrB_2Si_2O_8)$ of the Eu^{3+} *f*–*d* transition in $SrB_2Si_2O_8$ are calculated to be 149 nm via Eq. (1). The CT transition energy could be estimated through the empirical formula introduced by Jørgensen [55]:

$$E_{CT} = [\chi(X) - \chi(M)] \times 30\,000\ cm^{-1} \quad (2)$$

where E_{CT} gives the CT transition energy in cm^{-1}, $\chi(X)$ and $\chi(M)$ represent the optical electronegativity of the anion and the central metal ion, respectively. The O^{2-}–Eu^{3+} CT in $SrB_2Si_2O_8$ was determined to be 250 nm in Fig. 4. Using $\chi(Eu^{3+}) = 1.74$ [56], the $\chi(O)$ is calculated to be 3.073. Using $\chi(Ce^{3+}) = 1.07$ and $\chi(Tb^{3+}) = 0.95$ [56], the O^{2-}–Ce^{3+} and the O^{2-}–Tb^{3+} are estimated to be 167 and 157 nm, respectively. These excitations should be contained in the corresponding VUV excitation spectra although some of them may have been obscured. Note that the excitation profile of curve (d) in Fig. 8 is apparently different from those of curves (a)–(c). The difference can be interpreted that the stronger *f*–*d* transition of Tb^{3+} nearby 200 nm dwarfs the band within 165–190 nm range in curve (d).

6. Conclusions

$SrB_2Si_2O_8$ and $SrB_2Si_2O_8$:*RE* (*RE* = Eu^{3+}, Eu^{2+}, Ce^{3+}, Tb^{3+}) were successfully prepared via the conventional solid state reaction method in the present work. Parts of the Eu^{3+} in $SrB_2Si_2O_8$ were reduced to Eu^{2+} spontaneously even in air. The emission of the $SrB_2Si_2O_8$:Eu prepared in air can be switched between red and

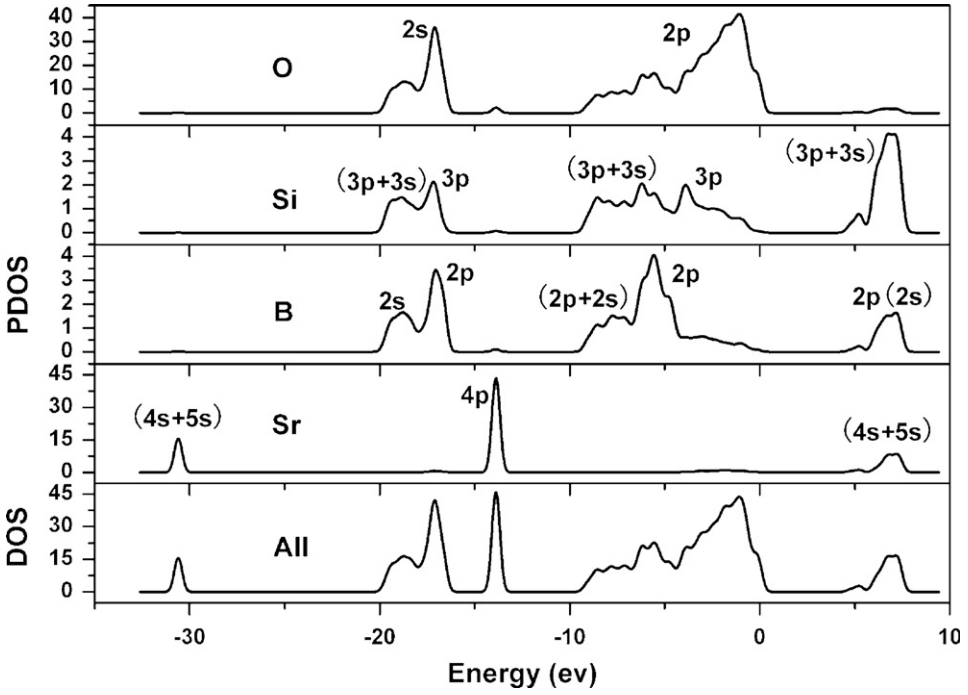

Fig. 11. DOS and PDOS plots of $SrB_2Si_2O_8$.

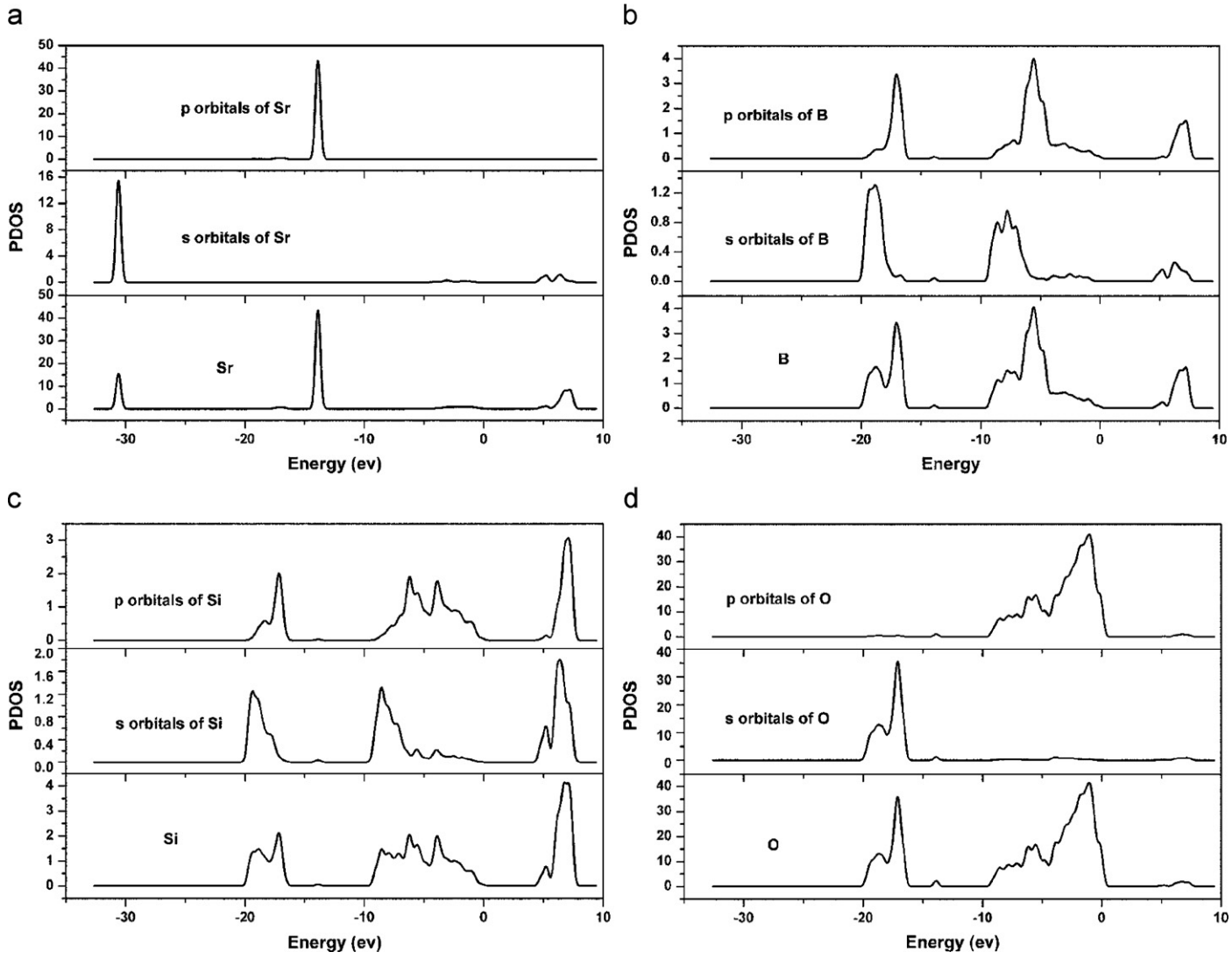

Fig. 12. Orbital-resolved PDOS of (a) Sr; (b) B; (c) Si; (d) O in $SrB_2Si_2O_8$.

blue by different excitation wavelengths. The Ce^{3+} and Tb^{3+} in $SrB_2Si_2O_8$ exhibited the blue and the green emissions at 396 and 541 nm, respectively. The *f-d* transitions of Ce^{3+} and Tb^{3+} in $SrB_2Si_2O_8$ were evaluated. The crystal field depression D (Ce^{3+}, $SrB_2Si_2O_8$) was determined to be 18 090 cm^{-1}.

The calculated direct LDA E_g for $SrB_2Si_2O_8$ was 4.27 eV. The computed DOS and PDOS indicated the valence band mainly was derived from the O 2*p* orbitals, with which the Si 3*p*(3*s*) and B 2*p*(2*s*) orbitals partly hybridized. Besides, the conduction band was composed of the Sr (4*s*+5*s*) orbitals together with the Si (3*p*+3*s*) and B 2*p*(2*s*) orbitals.

The VUV spectral characteristics of $SrB_2Si_2O_8$:*RE* (*RE* = Eu^{3+}, Eu^{2+}, Ce^{3+}, Tb^{3+}) were evaluated and discussed combining with the reflection spectrum and the calculated results. The host lattice absorption was assumed to be located in 165–200 nm. High energy states of the Ce^{3+} *f–d*, Tb^{3+} *f–d*, Eu^{3+} *f–d*, O^{2-}–Ce^{3+} CT and O^{2-}–Tb^{3+} CT were evaluated in the VUV excitation spectra.

Acknowledgments

This work was supported by the Program of New Century Excellent Talents in University of China (NCET, Grant no. 04–0978) and the Project of the Combination of Industry and Research by the Ministry of Education and Guangdong Province of China (Grant no. 0712226100023). We also thank Haining Cao for his efforts in the preparation for this paper.

References

[1] W.J. Weber, R.C. Ewing, C.A. Angell, G.W. Arnold, A.N. Cormack, J.M. Delaye, D.L. Griscorn, L.W. Hobbs, A. Navrotsky, D.L. Price, A.M. Stoneham, M.C. Weinberg, J. Mater. Res. 12 (1997) 1946.
[2] J.M.P.J. Verstegen, J.W. Ter Vrugt, W.L. Wanmaker, J. Inorg. Nucl. Chem. 34 (1972) 3588.
[3] M.W. Phillips, G.V. Gibbs, P.H. Ribbe, Am. Mineral. 59 (1974) 79.
[4] J.W. Downs, R.J. Swope, J. Phys. Chem. 96 (1992) 4834.
[5] R.F.W. Bader, Acc. Chem. Res. 8 (1975) 34.
[6] R.F.W. Bader, Phys. Rev. B 49 (1994) 13348.
[7] V. Luaña, A. Costales, P. Mori-Sánchez, A. Martin Pendás, J. Phys. Chem. B 107 (2003) 4912.
[8] M.L. Gaft, B.S. Gorobets, J. Appl. Spectrosc. (USSR) 31 (1979) 1488.
[9] P. Dorenbos, J. Lumin. 91 (2000) 155.
[10] E. van der Kolk, P. Dorenbos, C.W.E. van Eijk, A.P. Vink, C. Fouassier, F. Guillen, J. Lumin. 97 (2002) 212.
[11] P. Dorenbos, J. Phys. Condens. Matter 15 (2003) 575.
[12] U. Rambabu, S. Baddhudu, Opt. Mater. 17 (2001) 401.
[13] L. Wang, Y. Wang, J. Lumin. 122–123 (2007) 921.
[14] X.X. Li, Y.H. Wang, Mater. Chem. Phys. 101 (2007) 191.
[15] T. Berger, K.-J. Range, Z. Naturforsch. 51 (1996) 172.
[16] A.N. Belsky, J.C. Krupa, Displays 19 (1999) 185.
[17] S. Kubota, H. Yamane, M. Shimada, Chem. Mater. 14 (2002) 4015.
[18] Y. Wang, H. Gao, J. Solid State Chem. 179 (2006) 1716.

[19] J.L. Yuan, Z.J. Zhang, X.J. Wang, H.H. Chen, J.T. Zhao, G.B. Zhang, C.S. Shi, J. Solid State Chem. 180 (2007) 365.
[20] S.P. Feofilov, Y. Zhou, J.Y. Jeong, D.A. Keszler, R.S. Meltzer, J. Lumin. 125 (2007) 80.
[21] C. Cascales, R. Balda, V. Jubera, J.P. Chaminade, J. Fernández, Opt. Express 16 (2008) 2653.
[22] N. Kodama, Y. Watanabe, Appl. Phys. Lett. 84 (2004) 4141.
[23] N. Kodama, S. Oishi, J. Appl. Phys. 98 (2005) 103515-1.
[24] M. Yamaga, Y. Masui, S. Sakuta, N. Kodama, K. Kaminaga, Phys. Rev. B 71 (2005) 205102-1.
[25] P. Hohenberg, W. Kohn, Phys. Rev. 136 (1964) B864.
[26] W. Kohn, L.J. Sham, Phys. Rev. 140 (1965) A1133.
[27] CASTEP 3.5 program developed by Molecular Simulations Inc., 1997.
[28] M.C. Payne, M.P. Teter, D.C. Allan, T.A. Arias, J.D. Joannopoulos, Rev. Mod. Phys. 64 (1992) 1045.
[29] A.M. Rappe, K.M. Rabe, E. Kaxiras, J.D. Joannopoulos, Phys. Rev. B 41 (1990) 1227.
[30] J.S. Lin, A. Qteish, M.C. Payne, V. Heine, Phys. Rev. B 47 (1993) 4174.
[31] L. Kleinman, D.M. Bylander, Phys. Rev. Lett. 48 (1982) 1425.
[32] A.J. Read, R.J. Needs, Phys. Rev. B 44 (1991) 13071.
[33] R.W. Godby, M. Schluter, L.J. Sham, Phys. Rev. B 37 (1988) 10159.
[34] G. Bergerhoff, M. Berndt, K. Brandenburg, J. Res. Natl. Inst. Stand. Technol. 101 (1996) 221.
[35] K. Brandenburg, M. Berndt, J. Appl. Cryst. 32 (1999) 1028.
[36] Z. Pei, Q. Su, J. Zhang, J. Alloy Compd. 198 (1993) 51.
[37] J.R. Peterson, W. Xu, S. Dai, Chem. Mater. 7 (1995) 1686.
[38] H. Liang, H. He, Q. Zeng, S. Wang, Q. Su, Y. Tao, T. Hu, W. Wang, T. Liu, J. Zhang, X. Hou, J. Electron Spectrosc. Relat. Phenom. 124 (2002) 67.
[39] Q. Zeng, Z. Pei, S. Wang, Q. Su, Chem. Mater. 11 (1999) 605.
[40] H.-B. Liang, Q. Su, Y. Tao, T.-D. Hu, T. Liu, S.L.E. Shulin, J. Phys. Chem. Solid 63 (2002) 719.
[41] H. Liang, Y. Tao, Q. Su, S. Wang, J. Solid State Chem. 167 (2002) 435.
[42] Z. Pei, Q. Zeng, Q. Su, J. Solid State Chem. 145 (1999) 212.
[43] P. Dorenbos, Phys. Rev. B 65 (2002) 235110-1.
[44] L. Pidol, B. Viana, A. Kahn-Harari, A. Galtayries. A. Bessière, P. Dorenbos, J. Appl. Phys. 95 (2004) 7731.
[45] S. Saha, P.S. Chowdhury, A. Patra, J. Phys. Chem. 109 (2005) 2699.
[46] P. Dorenbos, J. Lumin. 87–89 (2000) 970.
[47] P. Dorenbos, L. Pierron, L. Dinca, C.W.E. van Eijk, A. Kahn-Harari, B. Viana, J. Phys. Condens. Matter 15 (2003) 511.
[48] P. Dorenbos, J. Lumin. 91 (2000) 91.
[49] K.C. Mishra, K.H. Johnson, B.G. Deboer, J.K. Berkowitz, J. Olsen, E.A. Dale, J. Lumin. 47 (1991) 197.
[50] C.H. Kim, I.E. Kwon, C.H. Park, Y.J. Hwang, H.S. Bae, B.Y. Yu, C.H. Pyun, G.Y. Hong, J. Alloy. Compd. 311 (2000) 33.
[51] A.V. Sidorenko, A.J.J. Bos, P. Dorenbos, C.W.E. van Eijk, A. K.-Harari, P.A. Rodnyi, B. Viana, Nucl. Instrum. Meth. Phys. Res. A 537 (2005) 81.
[52] Y. Hao, Y. Wang, J. Lumin. 122–123 (2007) 1006.
[53] Y. Wang, K. Uheda, H. Takizawa, U. Mizumoto, T. Endoa, J. Electrochem. Soc. 148 (2001) G430.
[54] Y. Wang, X. Guo, T. Endo, Y. Murakami, M. Ushirozawa, J. Solid State Chem. 177 (2004) 2242.
[55] C.K. Jørgensen, Prog. Inorg. Chem. 12 (1970) 101.
[56] Q. Su, J. Rare Earth. (special issue): Proceedings of the Second Conference on Rare Earth Development and Application, 1991, p. 765.